Acoustic imaging in confined and noisy environments using double layer Time Reversal and Field Separation Methods

Stéphanie Lobréau, Eric Bavu, Manuel Melon

7 - 12 SEPTEMBER 2014, KRAKÓW
FORUM ACUSTICUM

Acoustic imaging in confined and noisy environments using double layer Time Reversal and Field Separation Methods

Stéphanie Lobréau, Éric Bavu
Cnam Paris, LMSSC (EA3196), 292 rue Saint-Martin, F-75141 Paris Cedex 3, France.
Manuel Melon
LAUM UMR CNRS 6613, Avenue olivier Messiaen, F-72085 Le Mans cedex 9, France.

Summary
Many imaging methods cannot localize precisely unstationary sources in confined and noisy environments. In this paper, the use of a Time Reversal acoustic sink (TRS) method is proposed, in conjunction with a Field Separation Method (FSM). The proposed time reversal (TR) process is based on the measurement of the sound pressure field and its normal derivative on a double layer hemispherical antenna, which bounds the region of interest (ROI). These data are time-reversed and numerically back-propagated to a surface, 0.5 cm away from the source plane. As most imaging methods, the efficiency of this process relies on the use of the most suitable Green functions, which depend on the propagating environment. A way to improve the TR process is to transform numerically the confined space problem into a free field case, for which the Green functions are well-known. The proposed FSM consists in expanding the measured fields on the spherical harmonics functions, thus allowing to compute the outgoing waves. This process allows a precise localization and characterization of the source placed under the antenna, using free-field Green functions. Thanks to this method, the influence of reverberation and acoustic fields radiated by sources outside the ROI can be suppressed. The measurements presented in this paper are performed in an anechoic room, using two acoustic sources. The first one to image in the ROI emits a filtered pulse and the second one, placed outside the ROI, is driven by a Gaussian white noise. In order to assess the reconstruction quality of the proposed imaging process, a reference field is measured in an anechoic room on the back-propagation surface, corresponding to the pressure values when the source laying in the ROI is radiating alone. Comparisons with back-propagated pressures using TRS in conjunction with FSM show a good accuracy both in space and time domains.

PACS no. 43.60.Tj 43.28.We 43.60.Fg 43.58.-e

1. Introduction

TR imaging is a precise method, both in time and space domains, for unstationary sources localization. This process is based on an invariance principle [1]. In other words, considering the pressure field $p(\overrightarrow{r},t)$ as a solution of the waves equation, the time reversed pressure $p(\overrightarrow{r},-t)$ is a solution too. The accuracy of this imaging method relies on the Green function knowledge, which depends on the propagation medium. A way to improve the TR imaging process is to make it insensitive to the measurements environment. In this paper, we propose the use of a Field Separation Method (FSM), a technique based on the spherical harmonics expansions and on the use of double-layered antenna giving access to the complete acoustic field (p ; $\partial_n p$). This process separates the so-called "outgoing" field, which comes from the source to image, from the "perturbating" field, which is due to the noise source contributions and the environment influence [reverberation, reflections and/or diffraction from objects laying outside the region of interest (ROI)]. The main advantage of FSM is that this process transforms, numerically, the confined problem into a free-field case that makes possible to use TR imaging in any measurement environment.

2. Methods

2.1. Time reversal imaging

The TR process can be split into two phases (see Fig. 1). The first one consists in the measurement of the complete acoustic field $\left(p_m(\overrightarrow{r_s},t);\frac{\partial p_m(\overrightarrow{r_s},t)}{\partial n_s}\right)$ on a closed surface, called time reversal mirror (TRM) [2]. The second one is the numerical back-propagation of these data, which are time reversed, focusing back to the source position. The resolution of the TR imaging method depends both on the antenna aperture and on the frequency content of the source signal [1]. In an homogeneous medium and with a full aperture TRM, the width of the focal spot cannot be smaller than $\frac{\lambda}{2}$, where λ is the wavelength. This limitation is due to a diffraction phenomenon, corresponding to the

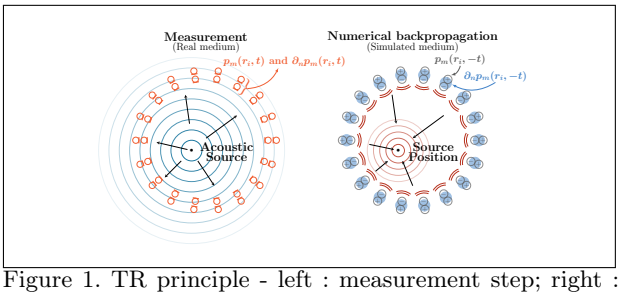

Figure 1. TR principle - left : measurement step; right : back-propagation of the time reversed data.

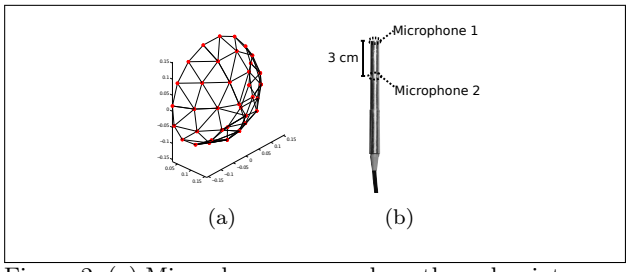

Figure 2. (a) Microphones array where the red points represent the probes position - (b) Two microphones spaced by 3 cm on the same probe

superposition of a convergent wave and a divergent one [3][4]. Complementary to the TR process, several methods have been proposed, such as MUSIC [5], DORT [6] or TR sink (TRS) [7]. In this paper, we propose to use a method based on the TRS which has the main advantage of improving the imaging resolution. This method consists in creating a numerical source which interferes with the divergent field created during the focusing step.

Using classical TR imaging, the time reversed field $p_{TR}(\overrightarrow{r},\text{-}t)$ can be reconstructed at each points $\overrightarrow{r}$ included in the volume delimited by the TRM via the Helmholtz-Kirchhoff integral. This equation depends on the knowledge of the Green function and its normal derivative (which are the propagators and thus are linked to the medium), and of the measurement of the pressure field and its normal derivative at $\overrightarrow{r_s}$, laying on the TRM :

$$p_{TR}(\overrightarrow{r},\text{-}t)=\iint_S \left[G(\overrightarrow{r_s},\overrightarrow{r},\text{-}t) * \frac{\partial p_m(\overrightarrow{r_s},\text{-}t)}{\partial n_s} - \frac{\partial G(\overrightarrow{r_s},\overrightarrow{r},\text{-}t)}{\partial n_s} * p_m(\overrightarrow{r_s},\text{-}t)\right] \mathrm{d}S$$

The efficiency of this TR imaging process obviously relies heavily on the Green function knowledge. If the measurement environment is free-field, the integral components can be computed as shown in the equations system (1), where $\cos(\gamma_s) = \frac{(\overrightarrow{r_s}\text{-}\overrightarrow{r}).\overrightarrow{n_s}}{|\overrightarrow{r_s}\text{-}\overrightarrow{r}|}$ and $\overrightarrow{n_s}$ is the normal vector to the measurement surface (S) :

$$\begin{cases} G(\overrightarrow{r_s},\overrightarrow{r},\text{-}t) * \dfrac{\partial p_m(\overrightarrow{r_s},\text{-}t)}{\partial n_s} = \dfrac{1}{4\pi|\overrightarrow{r_s}\text{-}\overrightarrow{r}|} \times \dfrac{\partial p_m\left(\overrightarrow{r_s};\text{-}t\text{-}\frac{|\overrightarrow{r_s}\text{-}\overrightarrow{r}|}{c}\right)}{\partial n_s} \\ \dfrac{\partial G(\overrightarrow{r_s},\overrightarrow{r},\text{-}t)}{\partial n_s} * p_m(\overrightarrow{r_s},\text{-}t) = \dfrac{cos(\gamma_s)}{4\pi|\overrightarrow{r_s}\text{-}\overrightarrow{r}|^2} \times p_m\left(\overrightarrow{r_s};\text{-}t\text{-}\frac{|\overrightarrow{r_s}\text{-}\overrightarrow{r}|}{c}\right) \\ \qquad\qquad + \dfrac{cos(\gamma_s)}{4\pi c|\overrightarrow{r_s}\text{-}\overrightarrow{r}|} \times \dfrac{\partial p_m\left(\overrightarrow{r_s};\text{-}t\text{-}\frac{|\overrightarrow{r_s}\text{-}\overrightarrow{r}|}{c}\right)}{\partial t} \end{cases} \quad (1)$$

In order to calculate the time-reversed back-propagated field, the use of monopolar and dipolar sensors is necessary. In our experiments, the transducers array is composed of pressure-pressure (p-p) probes with two microphones separated by 3 cm and arranged on a double layered hemispherical antenna (see Fig. 2 and Fig. 3(a)), giving access to $p_m(\overrightarrow{r_s},-t)$ and its normal derivative.

Since the complete acoustic field is measured on the antenna, two kinds of time reversal processes can be applied : TR focusing and TR imaging. TR focusing is an experimental approach and consists in replacing the microphones with loudspeakers radiating the time-reversed recorded data [4][8][9]. In that case, the more the propagation medium is random and/or reverberant the more the TR focusing is accurate [10]. In our case, we use an *imaging* process based on a back-propagation step in a simulated medium (Fig. 1). As seen before, TR imaging efficiency heavily depends on the propagators knowledge, which are accurate enough in free-field spaces, and fail if the medium is not modeled accurately enough [7].

Looking for a method which is usable whatever the propagation medium, we propose to apply a FSM. By separating the contributions coming from outside and inside the volume circumscribed by the antenna, this method can reconstruct the field which would have been measured in free-field, allowing the "denoising" of measured data and the use of the free-field Green functions G_0.

2.2. Field separation method

Several studies have already shown that FSM has the advantage to numerically change the confined problem to a free-field situation [11][12]. The method presented in this paper is mainly based on Weinreich's work [13]. Generally speaking, with the $e^{i\omega t}$ convention, a pressure field measured on a sphere of radius a can be mathematically expanded onto spherical harmonics functions basis using Eq. (2), where the acoustic pressure is $p(a,\theta,\phi)$, $h_n^{(2)}(ka)$ is the spherical Hankel function of the second kind, $j_n(ka)$ is the spherical Bessel function of the first kind and $Y_{nm}(\theta,\phi)$ is the spherical harmonics functions. The parameters α_{nm} and β_{nm} are the unknown quantities:

$$p(a,\theta,\phi) = \sum_{n,m} \left(\alpha_{nm} h_n^{(2)}(ka) + \beta_{nm} j_n(ka)\right) Y_n^m(\theta,\phi) \quad (2)$$

This pressure formulation separates inherently the radiation of the source to image, expressed using the Hankel function contribution, from the influence of the noise sources and the confined environment, expressed using the Bessel function contribution. In our measurements, the hemispherical array lays on a surface which is assumed to be perfectly rigid, thus allowing us to compute the complete acoustic field on an entire sphere being the union of the hemispherical array and its image mirror. Taking advantage of this symmetry, only half of the spherical harmonics are used (even $n+m$) . Using 36 p-p probes on the antenna, the expansion order is limited to $N=7$ [12].

Since we use p-p probes, we can assess the pressure field on two antenna layers whose radii are $a_1 = 14.5$ cm and

$a_2 = 17.5$ cm. The measured data are then expanded in the spherical harmonics basis :

$$\begin{cases} p(a_1,\theta,\phi) = \sum\limits_{\substack{n,m \\ (n+m)even}}^{n\leq m} \left(\alpha_{nm} h_n^{(2)}(ka_1) + \beta_{nm} j_n(ka_1)\right) Y_n^m(\theta,\phi) \\ p(a_2,\theta,\phi) = \sum\limits_{\substack{n,m \\ (n+m)even}}^{n\leq m} \left(\alpha_{nm} h_n^{(2)}(ka_2) + \beta_{nm} j_n(ka_2)\right) Y_n^m(\theta,\phi) \end{cases} \quad (3)$$

Solving this equations system (3) gives access to the quantities α_{nm} and β_{nm}, allowing to extract the acoustic field $p_{out}(\overrightarrow{r_s},\theta,\phi)$ of the source of interest, which would be measured in free-field without any perturbating sources.

The expansions on spherical harmonics is only valid if $ka_2 \leq N$. This condition introduces a cut-off frequency for the use of FSM, which is $f_c \approx 2180$ Hz for $a_2 = 17.5$ cm. A way to get a higher f_c consists in reducing the antenna radius, or alternatively in using more probes on the antenna. For the several further experiments, the signals used are accordingly low-pass-filtered with this cut-off frequency.

Thanks to FSM, knowledge of the propagation medium and of noise sources is unnecessary to perform TR imaging. Indeed, from the acoustic field measurements, the outgoing waves are separated from the incoming ones before being time-reversed and numerically back-propagated. As a consequence, the Helmholtz-Kirchhoff integral is applied with G_0 as propagator.

Based on velocity and pressure fields knowledge, a similar approach can also be used. These quantities can be obtained either with p-u probes or by computation on a hemisphere of radius $\langle a \rangle = \frac{a_1+a_2}{2}$ from the double layer antenna recordings. A previous study [12] shows that the performances of these two approaches are comparable, although the best results are obtained when the FSM technique matches with the probes type. In other words, to obtain the lowest separation errors, the p-p approach must be used with p-p probes. Likewise, p-u probes with the p-u approach.

2.3. Surfacic numerical integration

The use of TR-FSM imaging process requires the complete acoustic field $\left(p_m(\overrightarrow{r_s},t); \frac{\partial p_m(\overrightarrow{r_s},t)}{\partial n_s}\right)$ on a *closed* surface. Under the assumption that the source plane is perfectly rigid, the back-propagated field can be calculated using a surfacic integration on a *sphere* which corresponds to the union of the hemispherical measurement array and its mirror image. Surfacic integration on a sphere having been proved to be efficiently computed using Lebedev points and weights [14][15], we propose to compute the back-propagated acoustic field precisely using the Helmholtz-Kirchhoff integral and the use of $M = 86$ Lebedev nodes on the spherical surface (M depends on the spherical harmonics order N). The main idea is to propagate numerically the "denoised" field p_{out}, which is the result of the FSM process, to a larger sphere, in order to avoid edges effect during the integration process. The radius of this sphere is chosen to $a_{sph} = 65$ cm. The weighted field is then time-reversed and back-propagated to the imaging plane, 0.5 cm away from the source plane.

3. Error criterion

In order to assess the reconstruction quality, the computed field is compared to a reference pressure field measured at the same location. Several error indicators are used to quantify the differences between the reconstructed field and the reference one. The imaging method developed here must be accurate both in time and space domains. Therefore we use three error criterion [16]. The first and the second error criterion evaluate the spatial reconstruction quality. T_1 (Eq. 4) and T_2 (Eq. 5) are maps computed on each points (x_i, y_j) of the reconstruction plane and are respectively sensitive to phase and to magnitude differences. Ideally, $T_1 = 1$ and $T_2 = 0$, when no reconstruction errors occur.

$$T_1(x_i,y_j) = \frac{\langle p_{ref}(x_i,y_j,z_{ref},t) \times p(x_i,y_j,z_{ref},t)\rangle_t}{p_{ref}^{rms}(x_i,y_j,z_{ref}) \times p^{rms}(x_i,y_j,z_{ref})} \quad (4)$$

$$T_2(x_i,y_j) = \frac{\left|p_{ref}^{rms}(x_i,y_j,z_{ref}) - p^{rms}(x_i,y_j,z_{ref})\right|}{p_{ref}^{rms}(x_i,y_j,z_{ref})} \quad (5)$$

$p_{ref}(x_i,y_j,z_{ref},t)$ and $p(x_i,y_j,z_{ref},t)$ are respectively the time evolutions of the reference and the back-propagated field.

The time dependence quality of the back-propagated field is evaluated with the indicator E_n (eq. 6). The best value for this criterion is 0.

$$E_n(t) = \frac{\sqrt{\left\langle [p_{ref}(x,y,z_{ref},t) - p(x,y,z_{ref},t)]^2 \right\rangle_s}}{\left\langle p_{ref}^{rms}(x,y,z_{ref})\right\rangle_s} \quad (6)$$

4. Results

4.1. Experimental set-up

The results presented in this paper are assessed from measurements performed in an anechoic environment, with a source placed outside the ROI, that produces the pertubations of the acoustic field radiated by the main source. In the studied cases, we measure the pressure field studied on a hemispherical double-layered antenna, which consists of 72 phase and amplitude-calibrated pressure microphones mounted on 36 p-p probes.

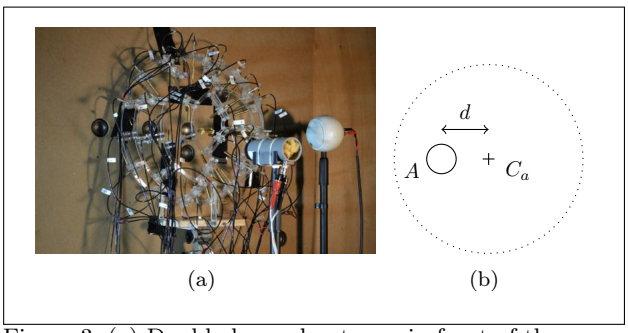

Figure 3. (a) Double-layered antenna in front of the moving baffled loudspeaker A (b) Loudspeaker A location in the source plane $z = 0$ and position of the antenna (dotted circle with a cross symbolizing the antenna center C_a)

The source plane is a rigid baffle with one 2" Aurasound loudspeakers mounted on it (see Fig. 3). The several sources are independently driven by filtered pulses signals using a M-Audio® external soundcard.

The acoustic field is measured at a sampling frequency of 32768 Hz, via a National Instruments® 96 channel PXI acquisition system controlled by the Labview® software.

4.2. Signal-to-noise ratio calculation

In this work, we investigate the influence of the signal-to-noise ratio (SNR) on the field reconstruction quality. We consider two positions for the source to localize : (1) centered ($d_1 = 0$ cm) and (2) off-centered ($d_2 = 10$ cm).

The SNR is expressed in dB using the main and the "perturbation" pressure fields, which are respectively denoted in Eq. (7) by p_s^{rms} and p_n^{rms}. These two quantities have been measured separately.

$$SNR = 20 \log \left(\frac{p_s^{rms}}{p_n^{rms}} \right) \tag{7}$$

In Eq. (7), RMS values are computed on a specific time-window. Since the emitted signal is unstationary and therefore contains many zeros, in contrast to the filtered white noise perturbation, measurements are windowed to only take into account the significant part of the "main" field for the SNR calculation. The window is defined from pressure level thresholds, chosen as a percentage of maximum outgoing field. Fig. 4 illustrates the windowing process. The light grey line is the white noise signal and the dark grey line is the pulse signal. From the thresholds (dashed black lines), chosen to be equal to ±2.5 % of the maximum magnitude of the signal source, the window can be defined. In other words, the SNR calculation is computed considering the time signal parts delimited by the two vertical black lines represented on Fig. 4.

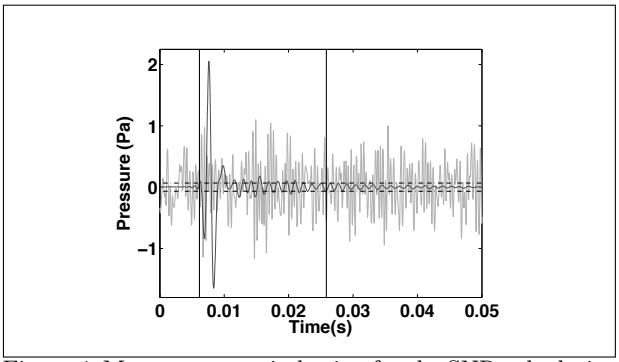

Figure 4. Measurement windowing for the SNR calculation

4.3. FSM efficiency

The first computation step in the TR-FSM process consists in removing the acoustic contributions coming from the outside the ROI. The results presented in Fig. 5 show the ability of the FSM method to retrieve the field which comes from the source to image for two SNR values. For $SNR = 10$ dB, the main source emission can be identified on the measurement (Fig. 5(a)), and FSM allows to retrieve efficiently and accurately the reference wave (Fig. 5(b)) by removing the perturbating field. For lower SNR value, such as $SNR = 0$ dB, the proposed method is still efficient at cleaning the measurements from perturbations. The reference field is retrieved (Fig. 5(d)), even if it is unnoticeable in the measured field (Fig. 5(c)) . The method begins to fail, though, for $SNR \leq -5$ dB (results not shown), which is understandable by looking at the measurements obtained for $SNR = 0$ dB.

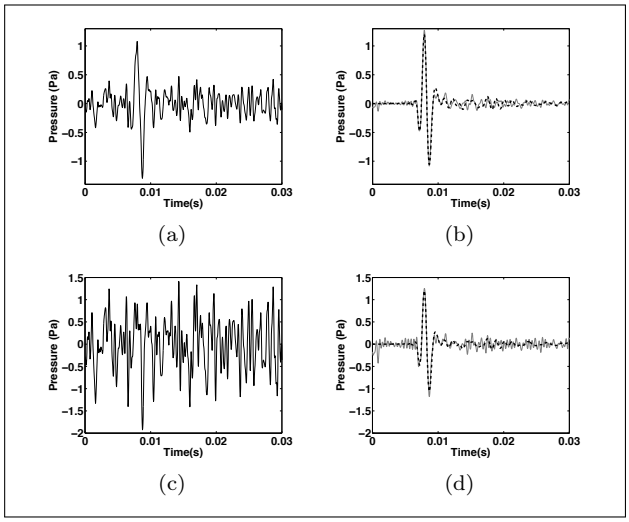

Figure 5. Time signals - Measurement with $SNR = 10$ dB (a) and $SNR = 0$ dB (c) - Comparison between the reference field (dashed line) and the reconstructed field with the FSM process (grey line) with $SNR = 10$ dB (b) and $SNR = 0$ dB (d)

4.4. Reconstruction of the main source emission

Thanks to FSM, the measurements are "denoised". Accordingly, the reverberant medium can be numerically changed into a free-field environment. The data are then time-reversed and back-propagated using G_0, focusing to the main source position.

4.4.1. Back-propagated field

Fig. 6 and Fig. 7 show the great interest of using the FSM process to suppress the acoustic perturbations and to compute the back-propagated field. When the source emission is masked or perturbated by noise contributions and when the FSM method is not used, the back-propagated field is composed by the main and the perturbations contributions, reducing drastically the TR imaging efficiency (Fig. 6(b), 6(c), 7(b) and 7(c)). That's why the use of FSM is essential to clean measurements and to have access to a more accurate localization of sources (Fig. 6(e), 6(f) , 7(e) and 7(f)).

These figures also highlight the collapse phenomenon described in section 2.1, limiting the resolution of the TR-FSM imaging method to $\frac{\lambda}{2} \simeq 14$ cm, the source signal frequency being centered at 1200 Hz. In these conditions, the main source can be localized, but not precisely (Fig. 6(e), 6(f) , 7(e) and 7(f)). When the SNR is at its limit of validity (0 dB), we begin to observe the perturbations influence on the reconstructed field (Fig. 6(f) and 7(f)). In other words, when the source noise energy is much more important than the main source contribution, TR-FSM begins to be sensitive to the perturbative contributions. In order to localize and characterize the source with high precision, we propose to improve the TR imaging resolution using a method based on the TRS [7].

4.4.2. Resolution improvement

TR-FSM resolution is limited by the superposition of convergent and divergent waves that can be mathematically

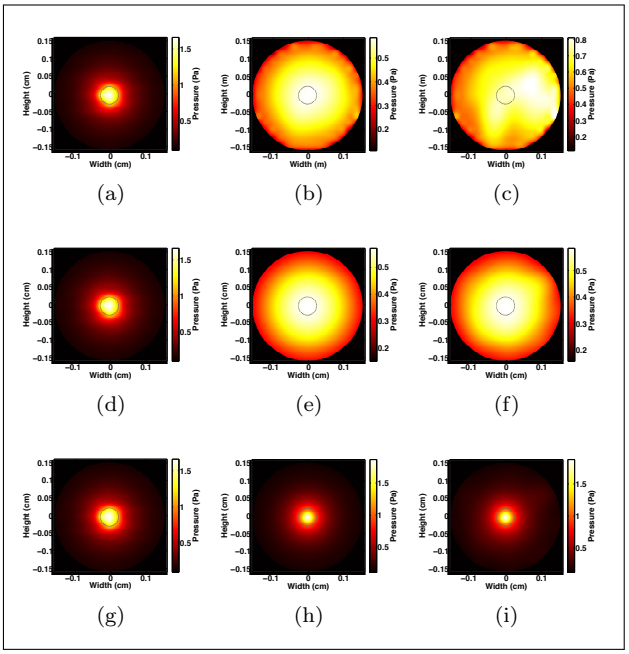

Figure 6. Reconstructed fields with TR imaging process when the main source is centered - Top : without FSM and without TRS : (a) reference field, (b) $SNR = 10$ dB, (c) $SNR = 0$ dB ; Middle : with FSM and without TRS: (d) reference field, (e) $SNR = 10$ dB, (f) $SNR = 0$ dB ; Bottom : with FSM and with TRS : (g) reference field, (h) $SNR = 10$ dB, (i) $SNR = 0$ dB

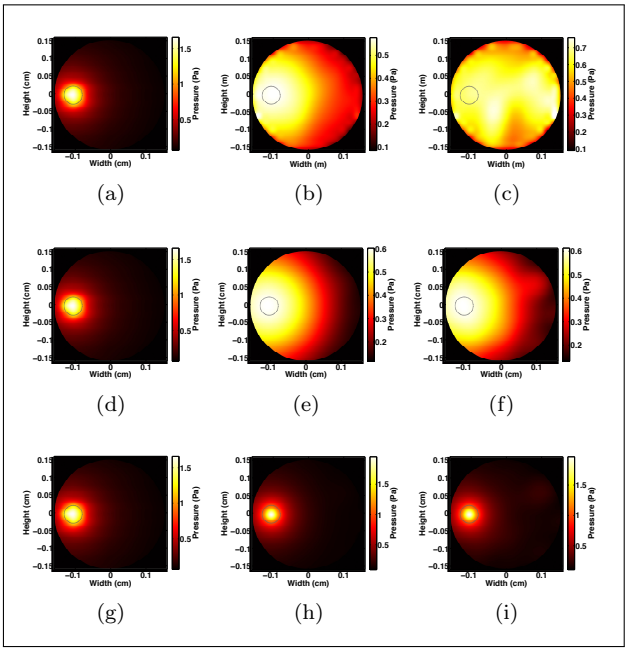

Figure 7. Reconstructed fields with TR imaging process when the main source is not centered - Top : without FSM and without TRS : (a) reference field, (b) $SNR = 10$ dB, (c) $SNR = 0$ dB ; Middle : with FSM and without TRS : (d) reference field, (e) $SNR = 10$ dB, (f) $SNR = 0$ dB ; Bottom : with FSM and with TRS : (g) reference field, (h) $SNR = 10$ dB, (i) $SNR = 0$ dB

expressed using Eq. (8), where $\overrightarrow{r}$ is a point of the imaging plane and $\overrightarrow{r_o}$ is the main source position.

$$p_{TR}(\overrightarrow{r}, -t) = p\left(\overrightarrow{r}, -t - \frac{|\overrightarrow{r_o} - \overrightarrow{r}|}{c}\right) - p\left(\overrightarrow{r}, -t + \frac{|\overrightarrow{r_o} - \overrightarrow{r}|}{c}\right) \tag{8}$$

Around the source position, Eq. (8) becomes :

$$p_{TR}(\overrightarrow{r}, -t) \underset{\overrightarrow{r} \to \overrightarrow{r_o}}{=} \frac{1}{4\pi c} \frac{\partial s(-t)}{\partial t} \tag{9}$$

where s is the signal emitted by the source to image.

The divergent part of Eq. (8) can be suppressed by emitting its exact opposite using a numerical sink [7]. This sink is positioned where the back-propagated pressure is at its maximum value and its emission signal is computed by integration of the extracted data at the sink position, according to Eq. (9).

The results of the TR-FSM process combined with the TRS show excellent agreements between the reference and the reconstructed fields (see Fig. 6(h), 6(i), 7(h) and 7(i)). At first sight, for the two considered SNR values, the source to image is well located and the pressure level of the back-propagated field corresponds very well with the reference one.

4.5. Reconstruction quality

In order to assess precisely the field reconstruction quality, we use the indicators defined before, T_1, T_2 and E_n. They are shown in Fig. 8 ($SNR = 10$ dB) and Fig. 9 ($SNR = 0$ dB) when the source to image is off-centered. These figures compare the classical TR imaging method using $\left(p_m(\overrightarrow{r_s}, t); \frac{\partial p_m(\overrightarrow{r_s}, t)}{\partial n_s}\right)$ quantities (top of the figures) with the results of the simultaneous use of FSM and TRS (bottom of the figures).

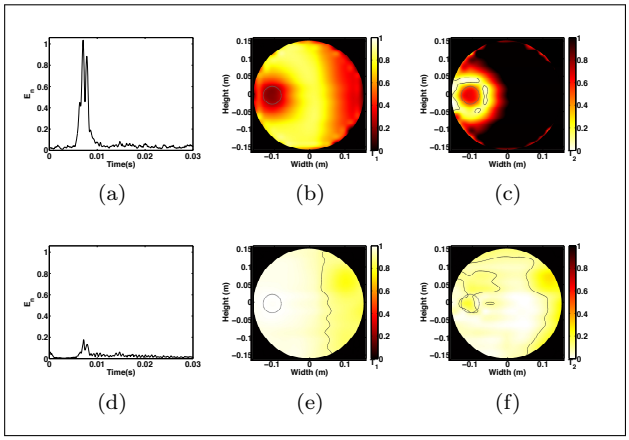

Figure 8. Error criterion for the off-centered source for $SNR = 10$ dB - Top : without FSM and without TRS : (a) $E_n(t)$, (b) T_1 map, (c) T_2 map; Bottom : with FSM and with TRS : (d) $E_n(t)$, (e) T_1 map, (f) T_2 map

The obtained results using only classical TR back-propagation (Fig. 8(a), 8(b), 8(c), 9(a), 9(b) and 9(c)) show that the pressure field is not accurately reconstructed on the imaging plane, due to external perturbations and due to the collapse phenomenon. E_n, T_1 and T_2 exhibit high error rates.

Thanks to FSM and TRS, external perturbations and limited resolution effects are suppressed. For the two SNR values, $E_n(t)$ time evolution exhibits a higher value when the source is radiating, but TRS and FSM methods allow

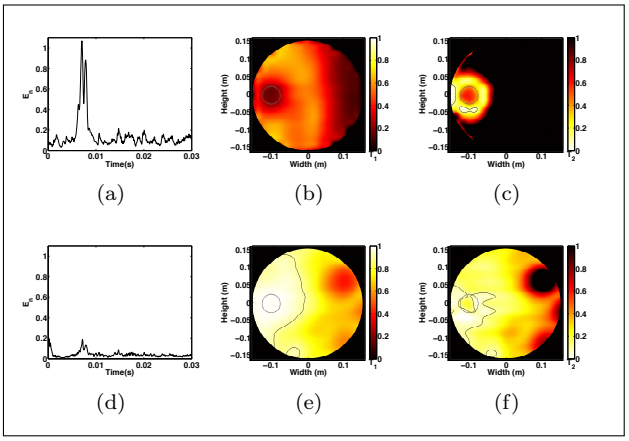

Figure 9. Error criterion for the off-centered source for $SNR = 0$ dB - Top : without FSM and without TRS : (a) $E_n(t)$, (b) T_1 map, (c) T_2 map; Bottom : with FSM and with TRS : (d) $E_n(t)$, (e) T_1 map, (f) T_2 map

to drastically reduce these errors (Fig. 8(d) and 9(d)).

When the FSM and TRS methods are used, T_1 maps (Fig. 8(e) and 9(e)) show that the shapes of the back-propagated pressure are precisely reconstructed nearby the main source position. T_2 maps (Fig. 8(f) and 9(f)) show an accurate back-propagated field computation on a large region around the source to image, that means the pressure levels aren't exactly recovered on the source location, but remain extremely satisfactory, especially for $SNR = 10$ dB. One can notice that T_1 and T_2 maps are degraded for $SNR = 0$ dB. In this case, the FSM process reaches its own performance limits : the back-propagated field is composed with the main source emission and the perturbations contributions that have not been filtered by FSM process. That's why the TR process efficiency decreases near the perturbative white noise source position, whereas this decreasing is not observed for $SNR = 10$ dB.

5. Conclusions

The imaging method presented in this paper is based on the measurement on a double-layered antenna of $\left(p_m(\overrightarrow{r_s},t); \frac{\partial p_m(\overrightarrow{r_s},t)}{\partial n_s}\right)$. Thanks to the use of a field separation method, based on spherical harmonics expansions, a double layer time-reversal imaging method can be used without any a-priori knowledge on the medium. This study shows that TR-FSM efficiency depends heavily on the ability of the FSM process to suppress the perturbations influence. We show that the method remains extremely accurate and succeeds, unless the main emission is totally masked by the noise contributions ($SNR \geq -5$ dB). The source to image is precisely localized and characterized. The resolution of the TR imaging process has also been improved using a numerical time reversal sink, taking advantage of the double layer measurements, thus giving an analytical formulation for the sink to introduce in this process. Precise comparisons with reference measurements in an anechoic room show that the proposed double layer TR imaging using FSM and TRS, allows reconstructing very accurately the pressure field of the source of interest in both time and space domains.

References

[1] M. Fink, D. Cassereau, A. Derode, C. Prada, P. Roux, M. Tanter: Time-reversed acoustics. Rep. Prog. Phys. **63** (2000) 1933-1995.

[2] M. Fink: Time Reversal of Ultrasonic Fields-Part I: Basic Principles. IEEE Trans. Ultrason., Ferroelect., Freq. Contr. **39** (1992) 555-566.

[3] J. de Rosny, M. Fink: Overcoming the Diffraction Limit in Wave Physics Using a Time-Reversal Mirror and a Novel Acoustic Sink. Phys. Rev. Lett. **89** (2002) 124301.

[4] E. Bavu, C. Besnainou, V. Gibiat, J. de Rosny, M. Fink: Subwavelength Sound Focusing Using a Time-Reversal Acoustic Sink. Acta Acust. United Ac. **93** (2007) 706-715.

[5] F. K. Gruber, E. A. Marengo, A. J. Devaney: Time-reversal imaging with multiple signal classification considering multiple scattering between the targets. J. Acoust. Soc. Am. **115** (2004) 3042-3047.

[6] N. Mordant, C. Prada, M. Fink: Highly resolved detection and selective focusing in a waveguide using the D.O.R.T. method. J. Acoust. Soc. Am. **105** (1999) 2634-2642.

[7] E. Bavu, A. Berry: Super-resolution imaging of sound sources in free field using a numerical time-reversal sink. Acta Acust. United Ac. **95** (2009) 595-606.

[8] S. Yon, M. Tanter, M. Fink: Sound focusing in rooms: The time-reversal approach. J. Acoust. Soc. Am. **113** (2003) 1533-1543.

[9] G. Ribay, J. de Rosny, M. Fink: Time reversal of noise sources in a reverberation room. J. Acoust. Soc. Am. **117** (2005) 2866-2872.

[10] A. Derode, A. Tourin, J. de Rosny, M. Tanter, S. Yon, M. Fink: Taking Advantage of Multiple Scattering to Communicate with Time-Reversal Antennas. Phys. Rev. Lett. **90** (2003) 014301.

[11] M. Melon, C. Langrenne, P. Herzog, A. Garcia: Evaluation of a method for the measurement of subwoofers in usual rooms. Acoustics J. Acoust. Soc. Am. **127** (2010) 256-263.

[12] Y. Braikia, M. Melon, C. Langrenne, E. Bavu, A. Garcia: Evaluation of a separation method for source identification in small spaces. J. Acoust. Soc. Am. **134** (2013) 323-331.

[13] G. Weinreich, E. Arnold: Method for measuring acoustic radiation fields. J. Acoust. Soc. Am. **68** (1980) 404-411.

[14] V. I. Lebedev: Values of the nodes and weights of quadrature formulas of Gauss-Markov type for a sphere from the ninth to seventeenth order of accuracy that are invariant with respect to an octahedron group with inversion. Zh. Vychisl. Mat. Mat. Fiz., **15** (1975) 48-54.

[15] C. Ahrens, G. Beylkin: Rotationally invariant quadratures for the sphere. Proc. R. Soc. A. **465** (2009) 3103-3125.

[16] S. Paillasseur, J.-H. Thomas, J.-C. Pascal: Regularization for improving the deconvolution in real-time near-field acoustic holography. J. Acoust. Soc. Am. **129** (2011) 3777-3787.